^{14}N(^{3}He,d)^{15}O as a probe of direct capture in the ^{14}N(p,γ)^{15}O reaction

P. F. Bertone, A. E. Champagne, M. Boswell, C. Iliadis, S. E. Hale, V. Y. Hansper, and D. C. Powell
University of North Carolina at Chapel Hill, Chapel Hill, North Carolina 27599-3255
and Triangle Universities Nuclear Laboratory, Durham, North Carolina 27708-0308
(Received 12 July 2002; published 27 November 2002)

Spectroscopic factors and asymptotic normalization coefficients (ANCs) have been determined for bound states in ^{15}O using the ^{14}N(^{3}He,d)^{15}O reaction. These results are used to calculate the astrophysical S factor for direct capture in the ^{14}N(p,γ)^{15}O reaction. We also discuss how uncertainties in optical-model parameters influence both the spectroscopic factors and the ANCs, and the effect that this has on the predicted direct-capture reaction rate.

DOI: 10.1103/PhysRevC.66.055804 PACS number(s): 25.40.Lw, 25.55.Hp, 26.20.+f, 98.80.Ft

I. INTRODUCTION

Stars more massive than about 1.5 times the mass of the sun produce energy during core hydrogen burning primarily via the CN cycle. In addition, the CN cycle is active in less massive stars near the end of this phase and in all stars on the red-giant branch. The typical temperatures in these environments are in the range $T \approx 0.02-0.08$ GK and here, the power produced by the CN cycle is limited by the rate of the slowest reaction, ^{14}N(p,γ)^{15}O. Previous measurements of the ^{14}N(p,γ)^{15}O reaction [1] indicate that the reaction mechanism at low energies includes contributions from resonant capture, direct capture, and from the tail of a subthreshold resonance at a center-of-mass energy $E_{\mathrm{c.m.}} = -504$ keV ($E_x = 6793$ keV). A recent measurement of the lifetime of the 6793-keV state [2] implies that the subthreshold resonance plays a relatively minor role, which is confirmed in a reanalysis of the (p,γ) data by Angulo and Descouvemont [3]. Nonetheless, the (p,γ) excitation functions show considerable structure, which complicates the extrapolation of experimental results to astrophysical energies. Therefore, it is useful to isolate the different reaction components using complementary techniques. For example, the direct-capture contribution can be examined separately through proton-stripping reactions. However, the only previous measurement of an absolute cross section for the ^{14}N(^{3}He,d)^{15}O reaction is from Artemov *et al.* [4], who report a spectroscopic factor and nuclear vertex constant for the ground state. Surprisingly, there have been no absolute measurements for any excited states. In this work, we have used the ^{14}N(^{3}He,d)^{15}O reaction to populate states in ^{15}O up to the lowest-lying (p,γ) resonance at $E_x = 7557$ keV ($E_{\mathrm{c.m.}} = 254$ keV). The extracted spectroscopic factors and asymptotic normalization coefficients (ANCs) can be used to calculate the cross sections for direct capture in ^{14}N(p,γ)^{15}O.

II. EXPERIMENTAL PROCEDURE AND RESULTS

A. Target production

A target of ^{14}N was produced by implanting singly charged ^{14}N ions into a 40-μg/cm^2 ^{nat}C foil. The foil was slackened by exposing it to a hand-held camera flash unit at a distance of 7 cm prior to ion bombardment, which minimized the chance that accumulated thermal stress would rupture the foil during implantation. The foil was placed directly behind a graphite collimator with a defining aperture of 1.27 cm. This was done so that carbon would be the only material sputtered onto the foil as a consequence of beam collimation. In addition, the carbon sputtered onto the target foil is thought to increase the lifetime of the foil during the implantation process [5]. A copper tube extended to within 2 cm of the target holder. It was cooled to liquid-nitrogen temperature in order to reduce the buildup of contaminants on the target, and biased to -90 V for suppression of secondary electrons from the target.

The implantation was performed at an energy of 45 keV using the Department of Physics & Astronomy ion implanter at the University of North Carolina. Beam currents were limited to 1.25 μA in order to keep the thermal stress within allowable limits. A target thickness of 2.2(2) μg/cm^2 was measured via Rutherford backscattering at $E_\alpha = 2$ MeV and at $\theta_{lab} = 130°-170°$.

B. Experimental details

A 20-MeV ^{3}He^{2+} beam was provided by the Triangle Universities Nuclear Laboratory FN tandem accelerator. Typical beam currents were between 100 and 150 pnA. The outgoing deuterons were momentum-analyzed using an Enge split-pole spectrometer and detected within a 42-cm long position-sensitive avalanche counter. The solid angle of the spectrometer was fixed at 2.0 msr in order to reduce the widths of the contaminant lines arising from carbon and oxygen in the target. Data were collected from $\theta_{\mathrm{lab}} = 5°$ to 22.5° in 2.5° steps and from 25° to 45° in 5° steps. Two momentum bites were required in order to observe states up to $E_x \approx 8$ MeV.

The composition of the target was monitored using a ΔE-E silicon telescope, mounted in the target chamber at $\theta_{\mathrm{lab}} = 44.2°$. No systematic evidence of nitrogen depletion was observed. Overall, the density of the target remained constant between runs, to an accuracy of 8%.

III. DATA ANALYSES

A. Angular distributions

Sample deuteron spectra collected at $\theta_{\mathrm{lab}} = 5°$ are shown in Fig. 1. Absolute cross sections were determined using the

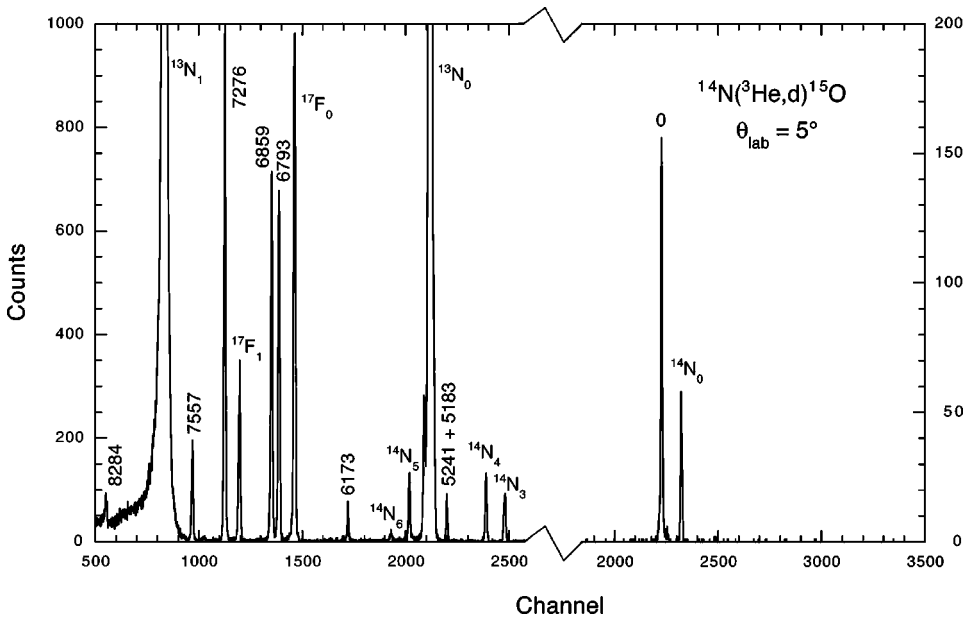

FIG. 1. Deuteron spectra, showing portions of two momentum bites, collected at $\theta_{lab}=5°$. Excitation energies are taken from Ref. [10]. The final states formed from carbon and oxygen contamination of the target are also labeled.

measured target thickness, the spectrometer solid angle, and the charge-collection efficiency derived from a previous measurement [6]. The uncertainty in the cross-section scale is 14.5%, which is dominated by the 10% uncertainty in the target thickness and a comparable uncertainty in our estimate of the charge-collection efficiency.

Theoretical differential cross sections were calculated with the distorted wave Born approximation (DWBA) code DWUCK4 [7]. A number of published optical potentials [8] for this mass and energy region were surveyed and few produced acceptable fits to the data. The quality of the fit was particularly sensitive to the choice of deuteron potentials and in general, those with no volume-imaginary and moderate surface-imaginary terms performed the best. Two sets of potentials (labeled I and II) produced fits of comparable quality that were superior to other combinations, and these are listed in Table I. In contrast, the choice of bound-state potential parameters is somewhat arbitrary. We have used parameters from an earlier study [4], but other choices could be easily justified. This ambiguity will introduce some model dependence in our final results, a point that we will discusss in some detail in Sec. IV A. Angular distributions and associated DWBA fits are shown in Fig. 2.

B. Spectroscopic factors

The relationship between the measured differential cross section, $d\sigma/d\Omega_{exp}$ and that calculated by DWUCK4, $d\sigma/d\Omega_{DWBA}$ is

$$\left(\frac{d\sigma}{d\Omega}\right)_{exp} = N\frac{(2J_f+1)}{(2J_i+1)(2j+1)}C^2S\left(\frac{d\sigma}{d\Omega}\right)_{DWBA}, \qquad (1)$$

where $N=4.42$ is an overall normalization [9], J_f and J_i are the spins of the final and initial states, respectively, and j is the transferred total angular momentum. Here we assumed $1p_{1/2}$, $2s_{1/2}$, $1d_{5/2}$, and $1f_{7/2}$ transfers. The quantity C^2S is the spectroscopic factor. The spectroscopic factors extracted from our data are listed in Table II. The values listed for each optical potential include a 1-σ uncertainty composed of contributions from statistics, target composition, and the DWBA fit. With the exception of the spectroscopic factors for the 5241-keV state and for the $l=3$ component of the 6176-keV state, the values obtained from the two optical potentials are in agreement and thus are combined in a weighted average to produce our recommended spectroscopic factors. The uncertainty in these final numbers also includes our uncertainties in the absolute cross-section scale and in the normalization

TABLE I. Optical-model parameters, using data from Ref. [8] unless noted otherwise.

Set	V_r	r_r	a_r	W_i	W_D	$r_i=r_D$	$a_i=a_D$	V_{so}	r_{so}	a_{so}	r_c
I: ^{3}He	130.0	1.07	0.79		9.17	1.67	0.72	4.0	0.96	0.79	1.30
I: d	107.5	0.884	0.915		6.55	1.593	0.684				1.30
II: ^{3}He	177.3	1.194	0.640	12.59		1.671	0.936				1.25
II: d	94.79	1.05	0.843		8.58	1.573	0.573	6.98	1.05	0.843	1.30
p[a]	[b]	1.30	0.70					$\lambda=25$			1.25

[a]Reference [4].

[b]Varied to match separation energy.

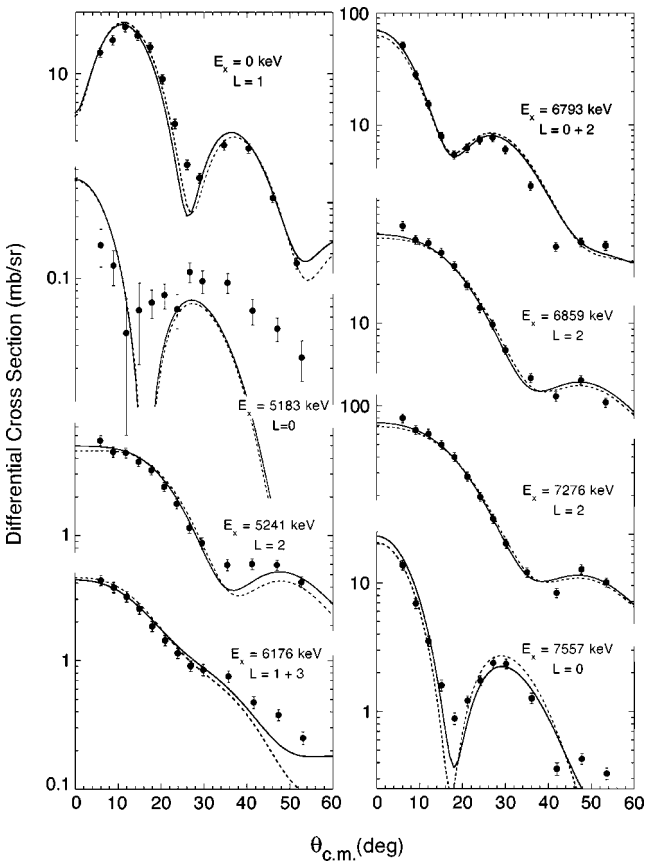

FIG. 2. Angular distributions and DWBA fits for the states of interest. The orbital angular momentum transfer is noted for each fit. The error bars represent statistical errors as well as the estimated relative uncertainty in the target density.

factor N. The latter source is usually not included in DWBA analyses and it is not clear what a reasonable estimate of the uncertainty would be. However, when the cross section is recast in terms of ANCs, an analogous term exists (as discussed below in Sec. III C) with a theoretical uncertainty of about 15% and we have adopted this same uncertainty for N. The normalization and absolute cross-section scale are the dominant contributors to the overall uncertainty in the recommended spectroscopic factor (and ANC). In contrast, the uncertainty arising from the choice of optical potential is negligible.

Spectroscopic factors reported in previous studies by Schröder *et al.* [1] and Artemov *et al.* [4] are also listed in Table II and there is good agreement with our results for most states. However, the agreement in the former case is surprising because they used very different bound-state potentials ($r_r = 1.7$ fm and $a = 0.7$ fm, versus $r_r = 1.3$ fm and $a = 0.7$ fm in the present study). If these parameters were used to analyze our data, then the resulting spectroscopic factors for the bound states would decrease by about a factor of 2.

To further test the reliability of our absolute cross-section scale and spectroscopic factors, we have estimated the proton width of the 7557-keV state using the relation

$$\Gamma_p = C^2S\,\Gamma_{\rm sp}, \tag{2}$$

where $\Gamma_{\rm sp}$ is the calculated proton width for a pure single-particle state. As discussed by Hale *et al.* [6], the product of C^2S and $\Gamma_{\rm sp}$ is quite insensitive to the bound-state parameters, provided that the same wave functions are used to calculate each quantity. Using our value of $C^2S = 0.82(18)$, we obtain $\Gamma_p = 1.04(23)$ keV, which is in excellent agreement with $\Gamma_p = 0.99(10)$ keV, obtained independently from (p,γ) measurements [1].

C. Asymptotic normalization coefficients

In situations where the reaction process is peripheral, which is often true for both direct-capture and stripping reactions, the reaction amplitude is mainly determined by the overlap integrals in the region external to the nucleus. In this

TABLE II. Summary of spectroscopic factors.

			C^2S			
E_x (keV)[a]	J^{π}[a]	l	Set I	Set II	Adopted	Literature[b]
0	$\frac{1}{2}^-$	1	1.8(2)	1.6(1)	1.7(4)	1.29(18), 1.4[c]
5183	$\frac{1}{2}^+$	0	0.0052(16)	0.0046(15)	0.0049(15)	0.004(1)
5241	$\frac{5}{2}^+$	2	0.083(7)	0.12(1)	0.094(20)	0.06(1)
6176	$\frac{3}{2}^-$	1	0.047(4)	0.054(5)	0.050(11)	0.038(16)
		3	0.075(7)	0.059(6)	0.065(14)	
6793	$\frac{3}{2}^+$	0	0.56(6)	0.48(5)	0.51(11)	0.49(1)
		2	0.15(2)	0.16(2)	0.16(3)	
6859	$\frac{5}{2}^+$	2	0.63(5)	0.59(5)	0.61(13)	0.37(1)
7276	$\frac{7}{2}^+$	2	0.69(5)	0.64(5)	0.66(14)	0.35(1)
7557	$\frac{1}{2}^+$	0	0.86(8)	0.78(7)	0.82(18)	0.78(8)[d]

[a]From Ref. [10].
[b]From the (p,γ) work of Ref. [1], unless otherwise noted.
[c]From the (^{3}He,d) work of Ref. [4].
[d]Calculated from $\Gamma_p = 0.99(10)$ keV (Ref. [1]).

case, the overlap integral $I_A^B(r)$ for $B \rightarrow A+p$ can be approximated by a Whittaker function:

$$I_A^B(r) \approx C_B \frac{W_{-\eta,l+1/2}(2kr)}{r}, \tag{3}$$

where W is the Whittaker function, η is the Sommerfeld parameter, l is the orbital angular momentum, and k is the wave number for the bound proton. For unbound states, the Whittaker function is replaced by the asymptotic form of the Gamow wave function [11]. The quantity C_B is the ANC for $B \rightarrow A+p$, which is related to C^2S via

$$C_B = (C^2S)^{1/2} b_B . \tag{4}$$

Here, b_B is the (calculated) ANC for the single-particle wave function $R(r)$:

$$R(r) \approx b_B \frac{W_{-\eta,l+1/2}(2kr)}{r}. \tag{5}$$

A more detailed discussion of the ANC technique can be found, e.g., in Ref. [12]. Within the ANC ansatz, the relationship between $d\sigma/d\Omega_{exp}$ and that calculated by DWUCK4 is

$$\left(\frac{d\sigma}{d\Omega}\right)_{exp} = \frac{(2J_f+1)}{(2J_i+1)(2j+1)} \frac{C_{15}^2}{b_{15}^2} \frac{C_3^2}{b_3^2} \left(\frac{d\sigma}{d\Omega}\right)_{DWBA}, \tag{6}$$

where C_{15} and C_3 are the ANCs for $^{15}O \rightarrow {}^{14}N+p$ and $^3He \rightarrow d+p$, respectively. The former is the ANC that we extract from our data, whereas the latter is determined [13] to be 3.9(6) fm^{-1}. The quantity b_{15} is the ANC for the $^{14}N+p$ bound-state wave function and $b_3^2 = |\langle d|^3He\rangle|^2$, which is the *s*-state probably for ^{3}He. An average of the results of 3-*N* calculations by Wu *et al.* [14] yields $b_3^2 = 0.898(9)$. The ratio C_3^2/b_3^2 is analogous to the normalization *N* used in extracting spectroscopic factors. The value here is 4.34(66) and we have applied the same relative uncertainty to *N*, as mentioned above.

To determine if our kinematics imply a reaction that is predominantly peripheral in nature, we have calculated the DWBA cross section, integrated over the region of the first maximum (specifically, from $\theta_{c.m.} = 0° - 20°$), for several values of the cutoff radius, which is the inner bound on the radial integral. These results are shown in Fig. 3 for the ground ($l=1$), 5183-keV ($l=0$), and 7276-keV ($l=2$) states. In all three cases, the major part (>90% on average) of the cross section arises from $r \geq 5$ fm. Since the combined interaction radii of $^3He+{}^{14}N$ is about 4.1 fm [15], the $^{14}N(^3He,d)^{15}O$ reaction is indeed peripheral at $E(^3He) = 20$ MeV. To minimize systematic uncertainties associated with our choices of optical-model parameters, we have extracted ANCs from the angular distribution at forward angles only ($\theta_{lab} \leq 15°$), and these are listed in Table III. However, these results would not change significantly if the full angular distributions were used instead. The uncertainties quoted in Table III were obtained in a manner analogous to that described above for the spectroscopic factors. In Table IV, we compare the spectroscopic factors derived from ANCs to the adopted values from Table II and in general, the agreement is excellent. Such consistency owes to the fact that we have used the same bound-state parameters for both the spectroscopic factors and the ANCs. This should not be surprising since, on a theoretical level, the ANC and the spectroscopic factor are related quantities [16]. However, the techniques used to extract them from the data are clearly different.

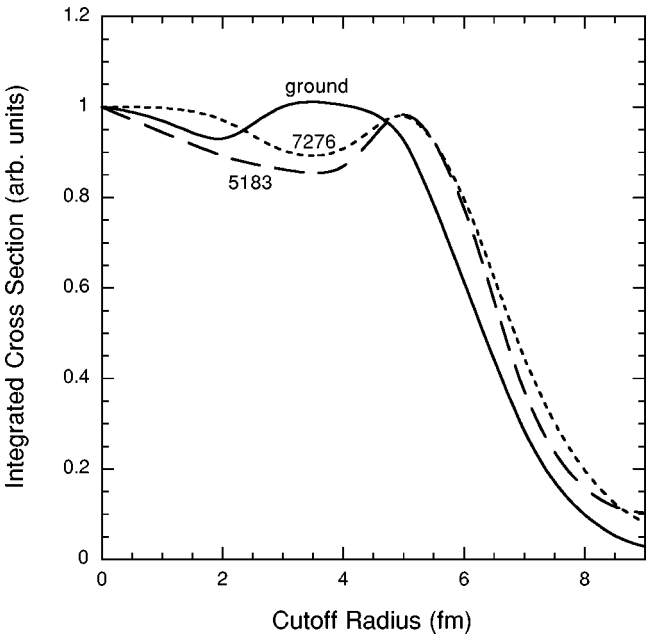

FIG. 3. Forward-angle cross sections, integrated over the range $\theta_{c.m.} = 0° - 20°$ as a function of cutoff radius for the ground, 5183-, and 7276-keV states.

IV. CONCLUSION

A. Systematic uncertainties

The spectroscopic factor in the DWBA is determined primarily within the nuclear interior and thus its value depends upon the parameters chosen for the bound-state potential, which are only weakly constrained by experiment. In contrast, the ANC (as derived from experimental data) is insensitive to the bound-state wave function by construction. The

TABLE III. Summary of asymptotic normalization coefficients.

		C_{15}^2 (fm^{-1})		
E_x (keV)	l	Set I	Set II	Adopted
0	1	58(4)	68(5)	63(14)
5183	0	0.11(3)	0.12(4)	0.11(4)
5241	2	0.12(1)	0.13(1)	0.12(3)
6176	1	0.44(4)	0.48(4)	0.46(10)
6793	0	21(2)	22(2)	21(5)
	2	0.083(8)	0.086(9)	0.084(19)
6859	2	0.35(3)	0.37(3)	0.36(8)
7276	2	$2.6(2)\times10^6$	$2.8(2)\times10^6$	$2.7(6)\times10^6$
7557	0	$3.2(3)\times10^{-4}$	$2.9(2)\times10^{-4}$	$3.1(7)\times10^{-4}$

TABLE IV. Comparison of spectroscopic factors.

E_x (keV)	l	C^2S [a]	C^2S [b]
0	1	1.7(4)	1.6(3)
5183	0	0.0049(15)	0.0028(9)
5241	2	0.094(20)	0.080(17)
6176	1	0.050(11)	0.086(19)
6793	0	0.51(11)	0.57(12)
	2	0.16(3)	0.17(4)
6859	2	0.61(13)	0.69(15)
7276	2	0.66(14)	0.72(16)
7557	0	0.82(18)	0.82(18)

[a]From Table II.
[b]Calculated from $C^2S = C_{15}^2/b_{15}^2$.

ANC technique is clearly a useful way of parametrizing a peripheral reaction [17]. To illustrate the effect of the bound-state parameters on both quantities, we have calculated spectroscopic factors and ANCs for two cases: a tightly bound state (the ground state) and a state that is slightly unbound (the 7557-keV state). The salient difference between these two extremes is that the wave function describing the former state is confined to the nuclear region, whereas the latter has a significant amplitude outside of the nucleus. The following radius and diffuseness parameters were used: $r_r = 1.15$, 1.25, 1.35, and 1.45 fm, and $a = 0.5$, 0.6, and 0.7 fm, and the entrance and exit parameters were taken from set II (Table I).

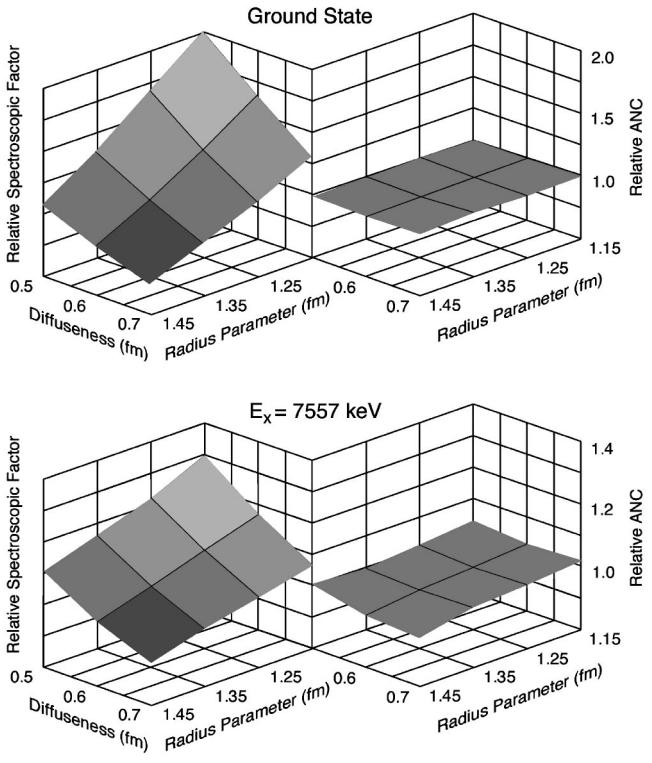

FIG. 4. Contour plots showing the relative variation in spectroscopic factors and ANCs for the ground and 7557-keV states, as a function of radius and difuseness.

The results are shown in Figure 4. The spectroscopic factor for the ground state varies over a factor of 2.78 for the 12 combinations of radius and diffuseness. In comparison, the corresponding ANC varies by a factor of just 1.03. Since the wave function for the 7557-keV state extends well beyond the nucleus, its spectroscopic factor is comparatively less sensitive to the bound-state potential. Here, the spectroscopic factor and ANC vary over factors of 1.39 and 1.08, respectively. Although the spectroscopic factor and ANC have similar experimental uncertainties, the former clearly has an inherently larger systematic bias. On the other hand, the ANC approach assumes a peripheral process, which must be verified on a case-by-case basis.

We emphasize that the spectroscopic factors and ANCs are only intermediate steps in calculating quantities of astrophysical interest, such as cross sections for direct capture or proton widths for resonances, and it is the uncertainties associated with the latter that are of more direct significance. Here, the spectroscopic factor or ANC acts as a scaling factor that relates a (theoretical) single-particle quantity to its physical counterpart, e.g.,

$$\sigma^{DC} = C^2S\,\sigma_{th}^{DC}; \quad \Gamma_p = C^2S\,\Gamma_{\rm sp}, \tag{7}$$

where σ^{DC} and σ_{th}^{DC} are the experimental and theoretical direct-capture cross sections, respectively, and $\Gamma_{\rm sp}$ is the aforementioned single-particle width. Analogous expressions using ANCs can be obtained by replacing C^2S with C_{15}^2/b_{15}^2. Both σ_{th}^{DC} and $\Gamma_{\rm sp}$ are determined near to or outside the nucleus: the overlap integral describing direct capture often reaches a maximum well outside the nuclear radius, while

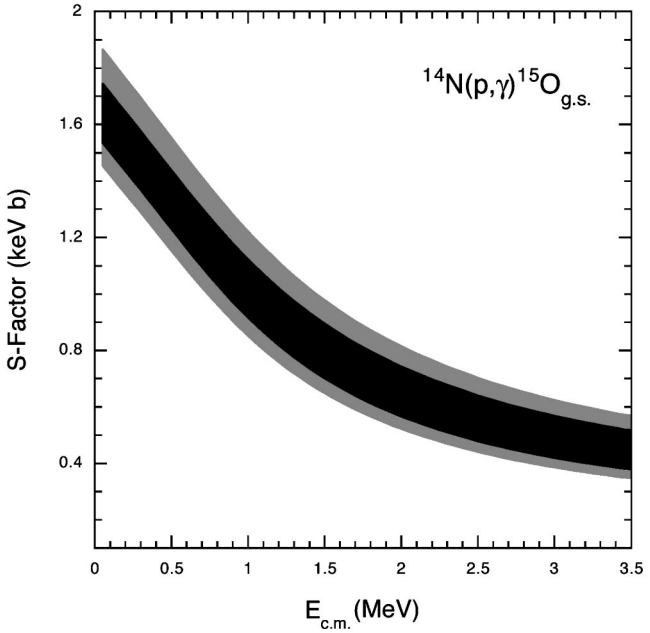

FIG. 5. S factor for direct capture to the ground state of ^{15}O calculated using the set II optical-model parameters. The dark band was calculated using the ANC for the ground state and shows the ± 1-σ variation for the ranges $r_r = 1.15$–1.45 fm and $a = 0.5$–0.7 fm. The lighter band indicates the same quantity obtained using the spectroscopic factor.

TABLE V. S-factor coefficients.

E_x (keV)	$S(0)$ (keV b)	$S'(E)$ (b)	$S''(E)$ (b/keV)
0	1.67(40)	-6.71×10^{-4}	7.42×10^{-7}
5183	$2.33(77)\times10^{-3}$	8.55×10^{-7}	-3.99×10^{-7}
5241	0.0110(26)	8.03×10^{-6}	-1.35×10^{-6}
6176	0.138(33)	-7.23×10^{-5}	1.45×10^{-5}
6793	1.17(28)	-6.94×10^{-4}	6.89×10^{-4}
6859	0.0349(84)	3.12×10^{-5}	2.46×10^{-6}
7276	0.0186(45)	3.81×10^{-5}	6.72×10^{-6}

$\Gamma_{\rm sp}$ depends on the values of the bound-state and Coulomb wave functions at the interaction radius. Thus, these quantities will vary with the choice of bound-state potential in the opposite direction as compared to spectroscopic factors, which depend more on the internal properties of the wave function. For example, a narrow, deep potential leads to a larger value for C^2S and a smaller value for σ_{th}^{DC} than would be the case for a wide, shallow potential. Another way to illustrate this point is to consider the proportionality

$$\sigma^{DC}=C^2S\,\sigma_{th}^{DC}\propto\frac{\left(\frac{d\sigma}{d\Omega}\right)_{\rm exp}}{\left(\frac{d\sigma}{d\Omega}\right)_{\rm DWBA}}\sigma_{th}^{DC}. \tag{8}$$

Changing the bound-state wave function will change both σ_{th}^{DC} and $d\sigma/d\Omega_{\rm DWBA}$ in the same direction. The ratio of these two quantities is therefore less sensitive to the bound-state potential. Clearly then, the systematic uncertainty in the product $C^2S\ \sigma_{th}^{DC}$ is much less than for C^2S alone. We illustrate this point in Fig. 5 in which the cross section for direct capture to the ground state, calculated with parameter set II and the various values for r_r and a listed above, is shown as a function of energy. Although C^2S varies by a factor of 2.78, the resulting maximum and minimum values of σ^{DC} differ by an average of 80% for $E_{\rm c.m.}=0.05-3.5$. MeV. The corresponding range using the ANC is 22%. The former deviation is still larger than the latter because for this case a sizeable portion of the direct-capture integrand comes from the nuclear interior. However, both deviations become smaller as the excitation energy increases. Note that these uncertainties are derived only from variations in r_r and a, and do not include any other sources of error. We have also calculated the proton width for the 7557-keV state and obtain 0.97(2) keV using C^2S and 1.10(2) using the ANC, which are consistent with each other and are of similar precision. Consequently, one might argue that the effects of uncertainties associated with spectroscopic factors have been overstated in the past. However, it is necessary to use the *same* bound-state wave function for σ_{th}^{DC} as for C^2S, which is often ignored and can lead to erroneous results. This requirement can be considerably relaxed when using ANCs. If the ANC technique is applicable, the results obtained from it are therefore more robust.

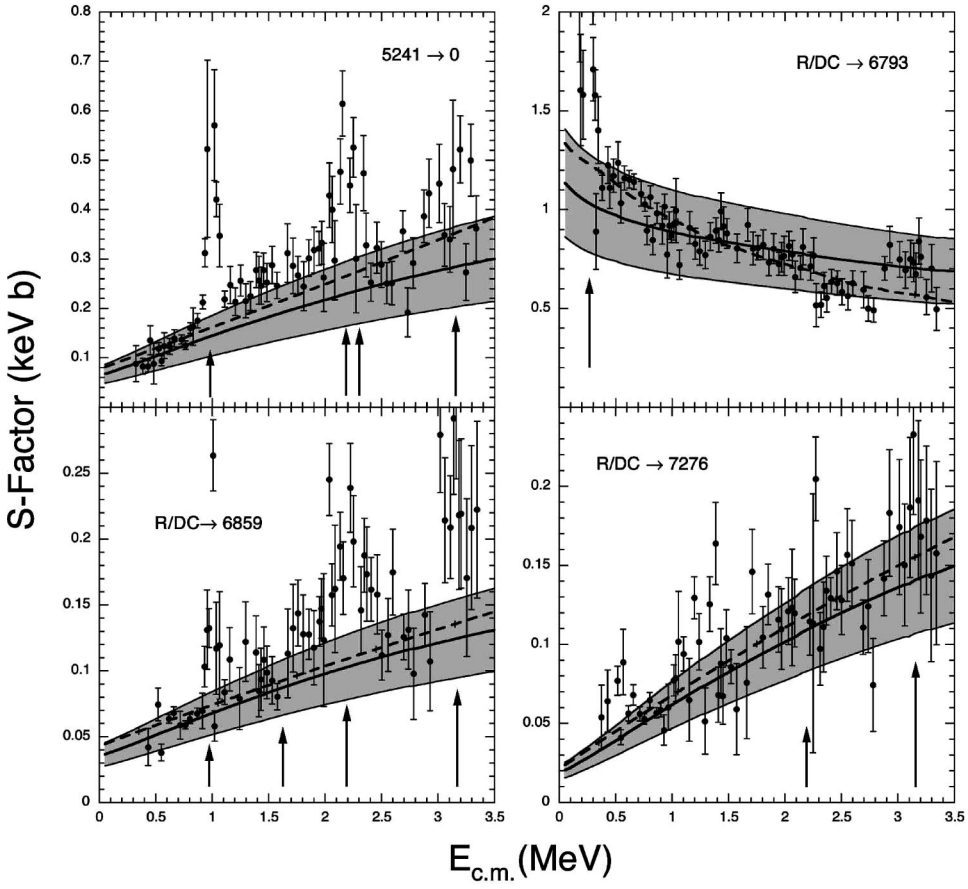

FIG. 6. S factors for selected transitions in the $^{14}{\rm N}(p,\gamma)^{15}{\rm O}$ reaction, taken from the data of Ref. [1]. The label R/DC refers to the fact that both resonances and direct capture can play roles in these transitions; the locations of expected resonances are indicated by the vertical arrows. Our predictions for the direct-capture component are indicated by the solid lines and the shaded areas represent the 1-σ uncertainties in our predictions. The dashed lines are the fits from Ref. [1] with resonances removed. Note that the 5241→0 transition results from several direct transitions, which have been combined in the solid curve.

B. Astrophysical aspects

We have calculated σ^{DC} for transitions leading to bound states in ^{15}O using the ANCs listed in Table III. The coefficients of second-order polynomial fits of σ^{DC}, valid for $E_{\text{c.m.}} \leqslant 750$ keV, are displayed in Table V. In assigning an uncertainty to $S(0)$, we have combined the uncertainties listed in Table III with an overall systematic uncertainty of $\pm 10\%$, which is a conservative estimate of the average uncertainty accompanying the choice of bound-state parameters for the states under consideration. The resulting overall uncertainty in $S(0)$ is typically 24% with the major contributions arising from the determination of the absolute cross section (14.5%) and from the uncertainty in C_3^2/b_3^2 (15.2%).

A comparison between our estimated S factor and the data of Schröder *et al.* [1] for the 5241→0 transition and capture into the 6793-, 6859-, and 7276-keV states are shown in Fig. 6. The other transitions are either dominated by resonances or the excitation functions are incomplete. Outside the resonance at $E_{\text{c.m.}} = 259$ keV, the strong transition to the 6793-keV state is well described by our result (the solid line is our prediction and the shaded area represents the ± 1-σ error band). It should be emphasized that our S factor is determined independently and does not represent a fit to the data. Our value for $S(0)$ [1.17(28) keVb] is somewhat lower than that of Ref. [1] [1.41(2) keVb]. However, this is mainly the result of the large radius used in their calculation of σ^{DC} (corresponding to $r_r = 1.7$ fm). Our prediction for the transition to the 7276-kev state also adequately represents the data. The values of σ^{DC} for the 5241→0 and R/DC→6859 transitions appear to underpredict the data. However, these transitions also have significant contributions from resonances. In general, our predictions are consistent with the *fits* from Schröder *et al.* [1] (the dashed curves in Fig. 6). Since the ^{14}N(p,γ)^{15}O reaction process is complicated by the interplay of resonances, direct capture, and interference effects at stellar energies, independent constraints on these quantities are an important means to ensure the accuracy of S factors derived from higher-energy data. The present work has provided reliable predictions of the direct-capture component of this reaction, which will improve the analysis and interpretation of the ^{14}N(p,γ)^{15}O excitation function.

ACKNOWLEDGMENT

This work was supported in part by US DOE Grant No. DE-FG02-97ER41041.

[1] U. Schröder *et al.*, Nucl. Phys. **A467**, 240 (1987).
[2] P.F. Bertone *et al.*, Phys. Rev. Lett. **87**, 152501 (2001).
[3] C. Angulo and P. Descouvemont, Nucl. Phys. **A690**, 755 (2001).
[4] S.V. Artemov *et al.*, Bull. Russ. Acad. Sci. Phys. **A60**, 1816 (1996).
[5] L.K. Fifield and N.A. Orr, Nucl. Instrum. Phys. Res. A **288**, 360 (1990).
[6] S.E. Hale *et al.*, Phys. Rev. C **65**, 015801 (2002).
[7] P. D. Kunz, computer code DWUCK4, University of Colorado, Boulder, CO, 1978 (unpublished).
[8] C.M. Perey and F.G. Perey, At. Data Nucl. Data Tables **17**, 1 (1976).
[9] R.H. Bassel, Phys. Rev. **149**, 791 (1966).
[10] F. Ajzenberg-Selove, Nucl. Phys. **A523**, 1 (1991).
[11] A.M. Mukhamedzhanov and R.E. Tribble, Phys. Rev. C **59**, 3418 (1999).
[12] A.M. Mukhamedzhanov *et al.*, Phys. Rev. C **63**, 024612 (2001).
[13] A.M. Mukhamedzhanov *et al.*, Phys. Rev. C **51**, 3472 (1995).
[14] Y. Wu *et al.*, Few-Body Syst. **15**, 145 (1993).
[15] N. Tanihata *et al.*, Phys. Lett. **160B**, 380 (1985).
[16] B.K. Jennings, Phys. Rev. C **62**, 027602 (2000).
[17] C.A. Gagliardi *et al.*, Phys. Rev. C **59**, 1149 (1999).